Probing Surface Chemistry Under Catalytic Conditions: Olefin Hydrogenation,Cyclization and Functionalization

Type of Report: Final Technical Report

Report Period: August 15, 2005 - August 14, 2008

Principle Author: Matthew Neurock

(and Wilfred T. Tysoe, University of Wisconsin, Milwaukee)

Date: May 26, 2011

DOE Award Number: DE-FG02-05ER15701

Name and Address of Submitting Organization:

Professor Matthew Neurock
Department of Chemical Engineering
102 Engineers' Way
University of Virginia
Charlottesville, VA 22904-4741

DISCLAIMER

ABSTRACT

The specific goal of this work was to understanding the catalytic reactions pathways for the synthesis of vinyl acetate over Pd, Au and PdAu alloys. A combination of both experimental methods (X-ray and Auger spectroscopies, low-energy ion scattering (LEIS), low-energy electron diffraction (LEED) and theory (Density Functional Theory (DFT) calculations and Monte Carlo methods under various different reactions) were used to track the surface chemistry and the influence of alloying. The surface intermediates involved in the various reactions were characterized using reflection-absorption infrared spectroscopy and LEED to identify the nature of the surface species and temperature-programmed desorption (TPD) to follow the decomposition pathways and measure heats of adsorption. These results along with those from density functional theoretical calculations were used determine the kinetics for elementary steps. The results from this work showed that the reaction proceeds via the Samanos mechanism over Pd surfaces whereby the ethylene directly couples with acetate to form an acetoxyethyl intermediate that subsequently undergoes a beta-hydride elimination to form the vinyl acetate monomer. The presence of Au was found to modify the adsorption energies and surface coverages of important surface intermediates including acetate, ethylidyne and ethylene which ultimately influences the critical C-H activation and coupling steps. By controlling the surface alloy composition or structure one can begin to control the steps that control the rate and even the mechanism.

Final Technical Report for DOE Grant, number DE-FG02-05ER15701

By

Matthew Neurock and Wilfred T. Tysoe

Department of Chemical Engineering, University of Virginia

Department of Chemistry and Laboratory for Surface Studies
University of Wisconsin-Milwaukee

Probing Surface Chemistry Under Catalytic Conditions: Olefin Hydrogenation,Cyclization and Functionalization.

1. Overall Progress

The project has focused on probing the reaction pathway for the catalytic synthesis of vinyl acetate from ethylene, oxygen and acetic acid represented stoichiometrically as:

$$C_2H_4 + CH_3COOH + \tfrac{1}{2}O_2 \rightarrow CH_3COOC_2H_3 + H_2O \quad (1)$$

and was first discovered about 40 years ago [1] and is catalyzed by palladium and palladium/gold alloys.

The project addresses two broad aspects of the chemistry:

A. Fundamental characterization of gold/palladium alloys.
B. Understanding reaction pathways on model single crystal metal and alloy surfaces.

A central and crucial component of this work is a close collaboration between theory (by the Neurock group) and experiment (by the Tysoe group) to provide insights into the structure of the alloys and into the reaction pathways and the effect that alloying might have on these.

1. (A) Characterization of the Alloy Structure

The central issues in fully characterizing the surface structure of the alloys are to understand the surface versus bulk composition of the alloy and how the gold and palladium atoms are distributed at the surface in order to make robust structure-function relationships. There are two principal methods for synthesizing model Au/Pd alloys. The first is to co-deposit films of gold and palladium onto a Mo(110) substrate and to anneal above ~800 K to form the alloy [2]. The second approach is to deposit several layers of gold onto a Pd(111) single crystal substrate and to heat to various temperatures to cause the gold to diffuse into the palladium bulk,

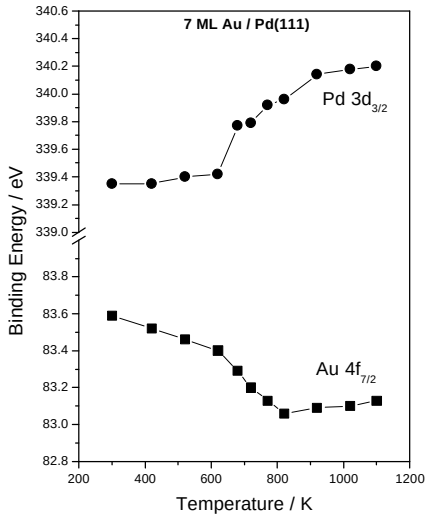

Figure 1: Plots of the Au $4f_{7/2}$ and Pd $3d_{3/2}$ binding energies of a Au/Pd(111) alloy as a function of annealing temperature.

thereby forming surface alloys [3,4]. While in the first case, the alloy film composition can be easily controlled by evaporating various amounts of each metal, it is rather tedious to grow films of various composition to synthesize each alloy. We have therefore elected to focus on the second strategy, which enables alloys of various structures to be obtained, merely by heating to increasingly higher temperatures [3,4]. Alloy formation can be measured using X-ray photoelectron spectroscopy and the changes in Pd $3d_{3/2}$ and Au $4f_{7/2}$ binding energies are displayed in Fig. 1 as a function of annealing temperature and reveal chemical shifts that are consistent with alloy formation. While one has to be very cautious in judging the net electron transfer during bimetallic alloying using photoelectron spectroscopy because of the rather complicated combination of initial and final state effects [5], the relative Pauling electronegativities of palladium (2.20) and gold (2.54) suggest that there should be a slight electron transfer from palladium to the gold, consistent with the observed chemical shifts. However, neither Auger spectroscopy nor XPS are sensitive only to the outermost layer composition since electrons can penetrate some way into the surface. Indeed, the substrate palladium Auger signal is only completely eliminated after about seven monolayers of gold have been deposited. This indicates that these surface-sensitive spectroscopies measure the composition of the outermost region of the sample, the selvedge. Thus, data such as that shown in Fig. 1 are not sensitive to subtle variations in composition at the surface so that the true composition of the outer surface may be different from that measured by these electron-based techniques. Low-energy ion scattering (LEIS) is sensitive to the composition of the outermost layer and LEIS experiments carried out on Au-Pd(111) alloys grown on a Mo(110) substrate have clearly demonstrated significant surface segregation of gold [2] and similar experiments have been carried out for gold-palladium alloys grown on a Pd(111) substrate. The results of this work are displayed in Fig. 2, where the bulk gold mole fraction was measured using Auger spectroscopy [6]. LEED intensity versus energy (I/E) curves were also measured for the alloy and yielded data in good agreement with that measured using LEIS [6]. If there were no preferential segregation, the graph would be a straight line. The most straightforward method for analyzing such data is to use a simple statistical

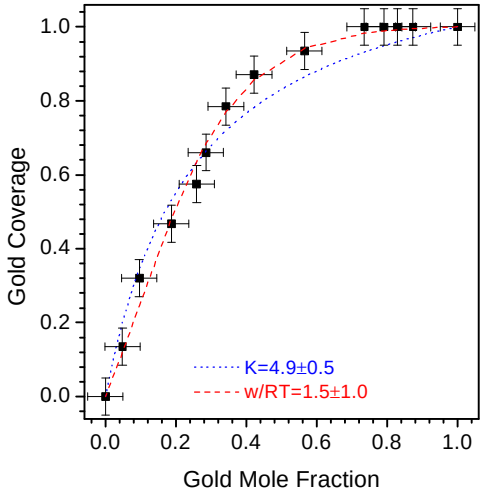

Figure 2: Plot of the gold coverage on a Au/Pd(111) alloy measured using LEIS versus the gold mole fraction in the bulk measured using Auger spectroscopy.

thermodynamic model for surface segregation with an energy difference for a gold atom in the bulk and on the surface yielding and equilibrium for segregation, *K*. This yields the Langmuir-McClean equation:

$$\Theta(Au) = \frac{KX(Au)}{1-(1-K)X(Au)} \qquad (2)$$

and a fit to equation (1) is shown as a dotted line in Fig. 2 yielding a value of K = 4.9 ± 0.5. A similar fit for alloys grown on a Mo(110) substrate [2] yield a value of 5.4 ± 0.2, in excellent agreement with the results for the alloy grown on a Pd(111) substrate.

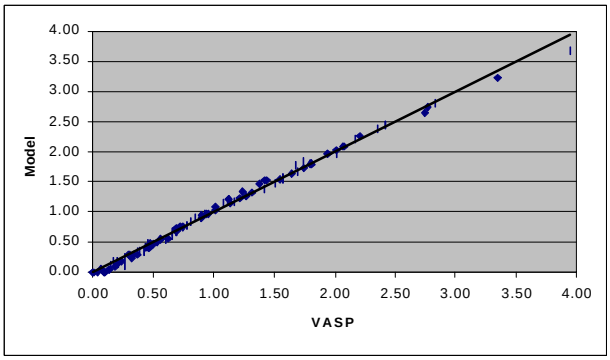

Figure 3: Comparison of the energies calculated using DFT for a Au/Pd(111) alloy with a model the assumes nearest-neighbor interaction between the gold and palladium atoms in the alloy.

While we plan to carry our scanning tunneling microscopy experiments on gold-palladium alloys, some work has already been carried out on Au/Pd(111) alloys [7,8] to measure the distribution of gold and palladium atoms on the surface [9]. In addition, recent density functional theory calculations suggest that there is a repulsive interaction between gold and palladium atoms in the surface. We have carried out similar DFT calculations for a range of alloys and fit the total energy to a model that includes nearest-neighbor interactions between atoms within the first and second layers, and between the atoms in the first and second layers [10]. The results of the comparison between the DFT calculations and the model are displayed in Fig. 3, where the agreement is excellent and yields a repulsive energy between gold and palladium atoms in the outermost layer of 0.06 ± 0.01 eV. This implies that, although no ordered LEED patterns are observed for the Au/Pd(111) alloy, this does not necessarily imply that the gold and palladium atoms are randomly ordered. In order to further explore this issue, we have carried out Monte Carlo calculations for gold palladium alloys as a function of values of *å*/kT, where *å* is the repulsive interaction energy between gold and palladium atoms in the surface. Typical results are displayed in Fig. 4, which plot the proportion of palladium monomers verus palladium coverage for a Au/Pd(111) alloy calculated using Monte Carlo simulations as a function of *å*/kT. This clearly shows a smooth transition in behavior with

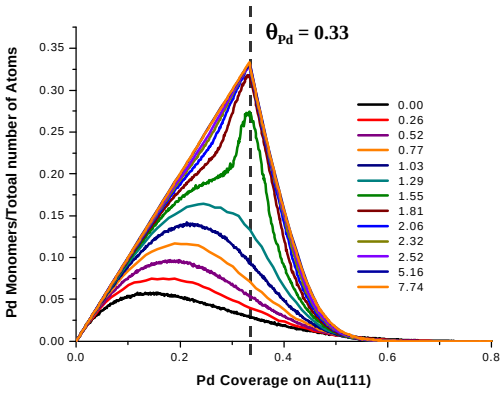

Figure 4: Plot of the number of palladium monomers versus palladium coverage as a function of increasing values of *å*/kT calculated using Monte Carlo methods.

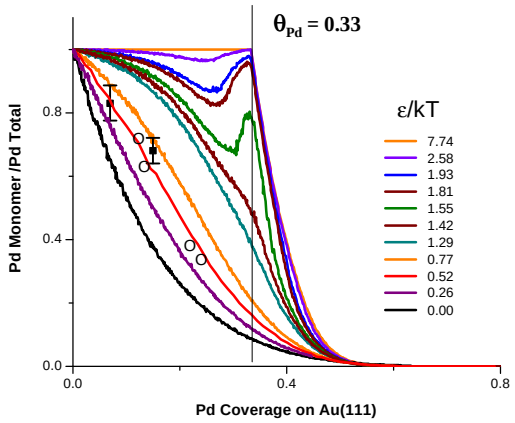

Figure 5: Comparison between the calculated proportion of isolated palladium atoms versus palladium coverage and the results of STM experiments.

increasing interaction energy, where for small values of interaction energy, no ordered structures appear, although there are a larger proportion of isolated sites than expected for a random distribution. Ordered surfaces appear above a critical interaction energy but are not necessarily perfectly ordered. The simulation results are compared with the results of experimental distributions of gold atoms measured by STM [7,8] and yields a value of *å*/kT of ~ 0.64 (Fig. 5). In particular, because of the repulsive interactions, the number of isolated palladium sites is approximately twice that which would be expected if they were randomly distributed. This difference will have an influence on the way in which active ensembles are identified on alloy surface to determine structure-function relationships. We are starting to explore this issue and have very recently examined the ensemble requirements for a very simple surface reaction, the formation of ethylidyne from ethylene on the Au/Pd(111) alloy surface. It is well known that ethylidyne forms a (2×2) overlayer on clean Pd(111) and adsorbs at three-fold hollow sites. It also exhibits an intense vibrational mode at ~1320 cm^{-1} that can be used to gauge the ethylidyne coverage (see below). We have measured the infrared spectra of ethylidyne on various Au/Pd(111) alloys and find a significant diminution in coverage when the alloy is formed. It is assumed that ethylidyne adsorbs on the alloy in a similar manner as on the clean surface, that is at three-fold hollow sites, but with the important additional condition that its coverage cannot exceed that of a (2×2) overlayer. The ethylidyne coverage is then calculated using a random sequential adsorption model and leads to predicted ethylidyne coverages on the alloy that are in extremely good agreement with experiment. This approach is still being developed, but we feel that it is essential to constructing robust structure-function relationships for realistic alloy surfaces that not only count active ensembles but can also take into account how adsorption on one site might influence the adsorption on neighboring sites.

1. (B) Surface and Catalytic Chemistry of Clean Pd(111) Surfaces

The structures of formate [11] and acetate species [12] have been measured on Pd(111) from their LEED I/E curves [13]. These experiments reveal that the carboxylate group bonds across a bridge site where the oxygen atoms are located approximately above palladium atoms with the OCO plane perpendicular to the surface and these measured structures are in very good agreement with those calculated by DFT. The structure of di-*s* -bonded ethylene has also been measured on Pd(111) using LEED, where this also occupies bridge sites [14].

One possible reaction pathway for VAM synthesis, first proposed by Samanos [15] suggests that reaction occurs between ethylene and acetate to form an acetoxyethyl intermediate,

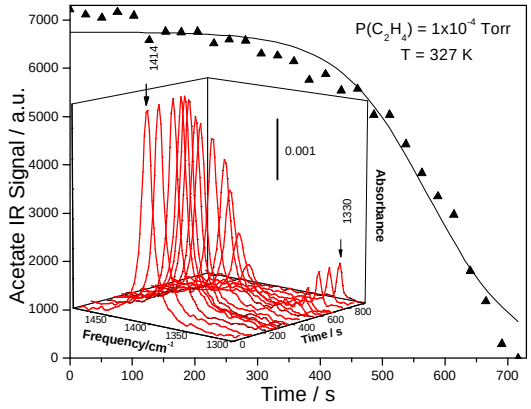

Figure 6: Plot of the integrated intensity of the 1414 cm^{-1} feature, due to acetate species, as a function of time. The lines plotted through these data are the results of a kinetic fit (see text). Shown also is the time sequence of infrared spectra of a saturated overlayer of acetate species on Pd(111)-(2×2)O pressurized by 1×10^{-4} Torr of ethylene at 327 K.

which decomposes by b -hydride elimination to yield VAM. Alternatively, recent theoretical evidence [16] indicates that ethylene could react to form a vinyl intermediate which then reacts with acetate to form VAM in a reaction pathway first proposed by Moiseev [17]. Theoretical calculations, however, indicate that the barrier for the activation of the C-H bond in ethylene to form adsorbed vinyl and hydrogen over Pd(111) is fairly high at 140 kJ/mol [14].

In order to explore the reaction pathway for the synthesis of vinyl acetate by a reaction between ethylene and surface acetate species, titration experiments were carried out in which an acetate-covered surface was pressurized with ethylene and the intensity of the strong OCO asymmetric stretching mode followed as a function of time [18,19]. It should be noted that adsorbing ethylene on an acetate-covered surface did not lead to reaction in TPD and merely resulted in the desorption of ethylene and decomposition of the acetate species. However, as shown in Fig. 6, there is a relatively rapid reduction in the intensity of the acetate infrared feature (at ~1414 cm^{-1}) when pressurized by ~1×10^{-4} Torr of ethylene at 327 K. The decrease in the acetate signal intensity confirms that acetate species react with ethylene and the plot (▲) shows the variation in intensity of the 1414-cm^{-1} acetate feature as a function of time. Another peak appears at ~1320 cm^{-1} as the acetate species have been removed assigned to ethylidyne formation on Pd(111) [19]. Calibration experiments show that the intensity of the 1414-cm^{-1} feature is proportional to the acetate coverage so that this plot represents a change in coverage of the acetate species as a function of time. This process can be modeled rather straightforwardly by assuming a second-order reaction between adsorbed acetate species (with coverage Θ) and adsorbed ethylene (coverage Θ_e) so that the reaction rate is given by:

$$-\frac{d\Theta}{dt} = k\Theta\Theta_e \qquad (3)$$

where k is the reaction rate constant. It is assumed that adsorbed acetate species block the adsorption of ethylene and this is to be expected based on the adsorbate structures [12,14] so that equation (3) becomes:

$$-\frac{d\Theta}{dt} = k\Theta\Theta_e^0(\Theta_0 - \Theta) \qquad (4)$$

where Θ_0 is the saturation acetate coverage and Θ_e^0 the saturation coverage of ethylene. Taking the initial acetate coverage at t = 0 to be $\Theta = \Theta_0 - d$ where d is an initial defect coverage yields:

$$\Theta = \frac{\Theta_0}{1 + \frac{d}{\Theta_0} e^{k't}} \qquad (5)$$

where $k' = k\Theta_0\Theta_e^0$. The line in Fig. 6 is a fit to equation (5) and reproduces the experimental data well, yielding a value of k'=1.4±0.1×10^{-2} s^{-1} at 327 K. It is further demonstrated using temperature-programmed reaction experiments carried out in UHV that this reaction results in the formation of vinyl acetate [18]. In order to further explore the reaction pathway, the reaction was carried out using various ethylene isotopomers (C_2D_4, CHDCHD and CH_2CD_2) and the results are displayed in Fig. 7. There is clearly strong isotope effect since reaction with C_2D_4 proceeds significantly more slowly than with C_2H_4 (by a factor of ~6). Interestingly, the two dideutero isotopomers also react with different rates and we will return to this issue below. Figure 8 displays a series of infrared spectra of the surface collected immediately after the acetate species had been removed by reaction with (b) C_2H_4, (c) C_2H_4 on a surface pre-covered by ^{18}O and (d) reaction with C_2D_4. Shown for comparison in (a) is a spectrum of a low coverage of carbon monoxide demonstrating that the other spectra are not due to background CO adsorption. Reaction with C_2H_4 (Figs. 8(b) and (c)) yields a feature at 1788 cm^{-1}, while after reaction with C_2D_4 the peak shifts to 1715 cm^{-1}. The additional peaks at ~1320 cm^{-1} are due to ethylidyne formation (compare with Fig. 5) [20-26]. The most obvious assignment of the 1715-cm^{-1} peak is to an isotope shift due to reaction with perdeuterated ethylene. In order to test this idea, both vinyl acetate and perdeuterated vinyl acetate were adsorbed on an ethylidyne-covered Pd(111) surface and both yielded peaks at 1788 cm^{-1}. As will be shown below, vinyl acetate decomposes when adsorbed on clean Pd(111) so that the ethylidyne species serve to stabilize the vinyl acetate that is produced. In the Moiseev pathway [17], where VAM is proposed to form directly by reaction between a vinyl species and an acetate, the only

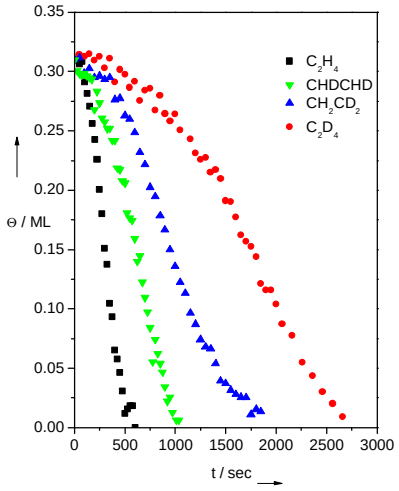

Figure 7: Plot of the acetate coverage as a function of time when reacting with various isotopomers of ethylene.

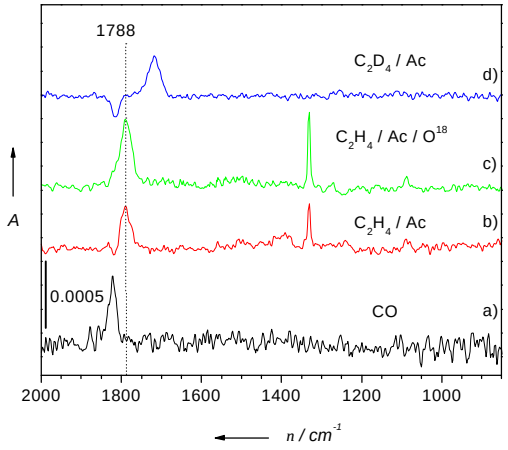

Figure 8: Infrared spectra of acetate species reacted with ethylene at 327 K until the acetate species had been removed, for reactions with (b) C_2H_4 with acetate-covered Pd(111), (c) C_2H_4 with acetate-covered ^{18}O-(2×2)/Pd(111) (d) C_2D_4 with acetate-covered Pd(111). Shown for comparison is the infrared spectrum of CO on Pd(111) (a).

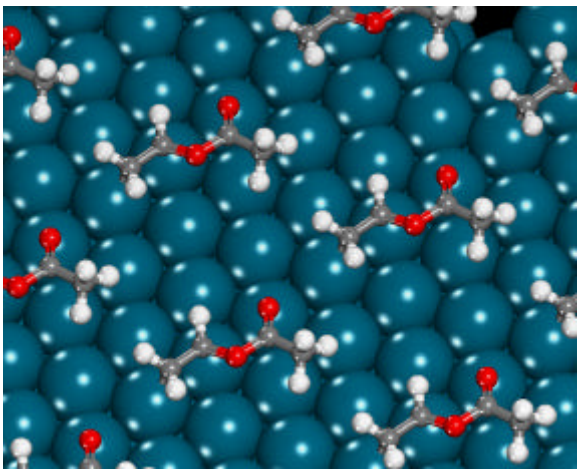

Figure 9: Depiction of vinyl acetate adsorption on a clean Pd(111) calculated using density functional theory [28].

participating species are acetate, ethylene, vinyl and vinyl acetate, and the 1715-cm^{-1} feature is due to none of these. However, in the Samanos route, the reaction is proposed to proceed via an acetoxyethyl-palladium intermediate [15]. DFT calculations show that the structures of the acetoxyethyl intermediate and vinyl acetate are characteristically different in their orientation and bonding of the OCO group to the Pd surface. The acetate group is strongly bound in a perpendicular orientation to the surface in the acetoxyethyl. The acetate group in the adsorbed vinyl acetate, however, is oriented parallel to the surface and is simply a substituent, which interacts weakly with the surface. DFT calculations of the vibrational modes of the adsorbed acetoxyethyl intermediate show that it has an intense C-O stretching mode at ~1715 cm^{-1} [18], and it is well known that the C-O stretching frequency in ethyl acetate is lower than that in vinyl acetate [27] so that the feature at ~1715 cm^{-1} is assigned to the acetoxyethyl-palladium intermediate, consistent with the Samanos pathway. This accumulates when C_2D_4 is used as reactant since its decomposition is slowed due to the presence of deuterium on the b carbon, which has a much slower decomposition rate than the hydrogenated analog (see Fig. 7). This also allows the data in Fig.7 to be understood in the context of this pathway. This observation allows us to immediately exclude the Moiseev model since, in this case, the rate-limiting step, which involves hydrogen, must be hydrogen abstraction from ethylene to form the vinyl species. A fit to the experimental data yields value of k(H)/k(D) ~ 6, a reasonable value for a primary isotope effect. In the case of reaction with d_2-ethylene, according to the Moiseev pathway, the rate constant should be (k(H)+k(D))/2, irrespective of the location of deuterium, yielding an isotope effect of 2/(1+(k(D)/k(H)) ~ 1.7. At first sight, a similar effect should occur with the Samanos model. In the case of reaction with CH_2CD_2, there is an equal probability of CH_2 or CD_2 being at the b -position in the acetoxyethyl-palladium intermediate, yielding an isotope effect of ~ 1.7, while for CHDCHD there will always be a CHD group at the b -position, similarly yielding an isotope effect of ~1.7. However, if the acetoxyethyl-palladium intermediate blocks the adsorption of ethylene, any intermediates formed from CH_2D_2 with two deuteriums in the b -position will decompose more slowly than those with hydrogens at that position, blocking ethylene adsorption and slowing the reaction rate. For reaction with CHDCHD, hydrogen will always be present at the b -position, so that the intermediate decomposes more rapidly, resulting in less blocking of ethylene adsorption by the intermediate. This suggests that reaction with CH_2CD_2 should be slower than that with CHDCHD as found experimentally (Fig. 7). This proposal is in accord with the observation of the acetoxyethyl-palladium intermediate identified for reaction between acetate species and C_2D_4 (Fig. 7). In this case, there is always a deuterium at the b -position resulting in slower decomposition of the

acetoxyethyl-palladium intermediate allowing it to be detected by infrared spectroscopy. The fact that this is detected confirms that sufficient intermediate can accumulate on the surface to affect the relative reaction rates of 1,1- and 1,2-dideuteroethylene as found in the data of Fig. 6. As a final check on these conclusions, DFT calculations were carried out for both the Moiseev and Samanos models. These show that the activation energies of elementary steps of the Moiseev pathway are nearly two times higher than for the Samanos pathway in accord with the experimental conclusions above. These calculations also reveal that the activation energy for ethylene insertion to form the acetoxyethyl-palladium intermediate is 73 kJ/mol and that for b -hydride elimination (the rate-limiting step) is 60.7 kJ/mol. The activation energy for this step was measured experimentally by carrying out titration experiments such as those shown in Fig. 5 as a function of temperature yielding an experimental activation energy of 55± 6 kJ/mol. This firstly suggests that DFT calculations are capable of yielding reliable activation energies, and second provides further confirmation that the reaction proceeds via the Samanos pathway. These results will provide a basis for studying this reaction on alloy surfaces and for understanding the enhanced selectivity of this surface.

As part of this work, we have also studied the chemistry of vinyl acetate on clean Pd(111) using RAIRS and TPD [28]. In this case, a portion of the vinyl acetate desorbs molecularly with an activation energy, measured from TPD, of 65 ± 7 kJ/mol. The structure of vinyl acetate was also calculated using DFT and the most stable structure is depicted in Fig. 9. The calculated heat of adsorption is 63.4 kJ/mol, in excellent agreement with the measured value. In addition, the relative intensities of the VAM vibrational modes are in accord with the structure shown in Fig. 9. Adsorbed vinyl acetate thermally decomposes on clean Pd(111) and the decomposition pathways

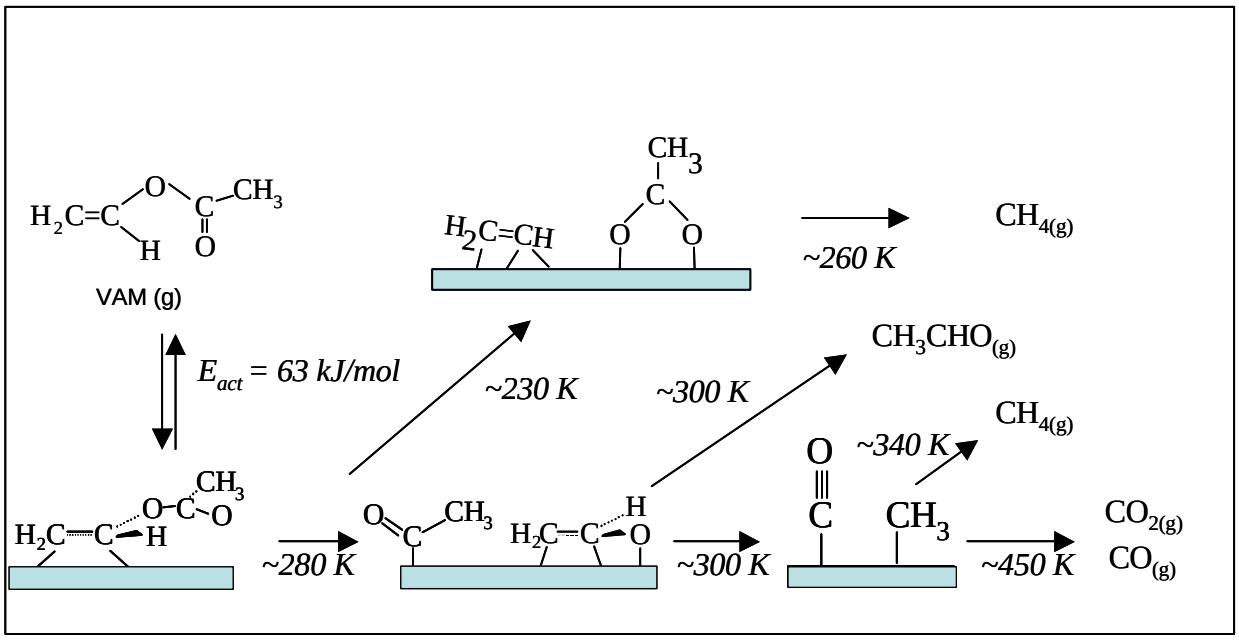

Figure 10: Schematic depiction of the decomposition pathways of vinyl acetate on clean Pd(111)

are summarized in Fig. 10. It should be noted that VAM appears to be stable on an ethylidyne-

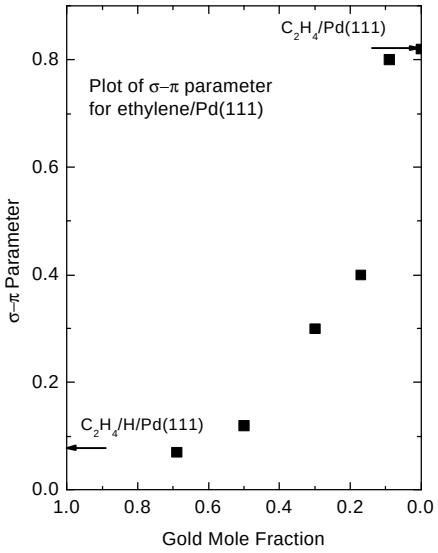

Figure 11: Plot of $s - p$ parameter for ethylene on various Au/Pd(111) alloys as a function of gold concentration in the near-surface region.

covered surface and this inhibition effect will be studied further.

1. (C) Surface and Catalytic Chemistry on Au/Pd(111) Alloy Surfaces

Experiments have been carried out to study the surface chemistry of reactants on model Au/Pd(111) alloys as a function of alloy composition. In all of the following cases, the alloy composition is measured using either Auger spectroscopy or XPS and therefore represents the composition of the near-surface region of the alloy sample, not the composition of the outermost layer. Now we have measurements of the gold coverage and distribution (see above), the data will be analyzed in terms of the surface coverage. The surface chemistry was characterized using a combination of TPD and RAIRS. The formation of an alloy resulted in a drastic change in the properties of ethylene as a function of alloy composition. The degree of ethylene hybridization can be gauged using the "$s - p$" parameter [29], define to be zero for ethylene in which the carbon is sp^2 hybridized and unity for a species in which the carbon is sp^3 hybridized. This parameter can be estimated using infrared spectroscopy and the resulting values of $s - p$ parameter are plotted versus alloy composition in Fig. 11 [30] and shows that the $s - p$ parameter varies from less than 0.1 to ~0.8 as the palladium content in the alloy increases. Similar trends are seen in the chemistry of acetic acid on Au/Pd(111) alloys [31]. Acetic acid adsorbs molecularly on a Au/Pd(111) alloy surface for gold concentrations in the alloy greater than ~0.33. The acetic acid desorbs with an activation energy of ~50 kJ/mol and forms catemers on the surface, particularly when the gold concentration is large. When the gold concentration is less than ~0.33, adsorption of acetic acid at 80 K and heating to ~210 K forms h^1-acetate species on the surface. On further heating, these can either thermally decompose to eventually evolve hydrogen, water and oxides of carbon, or form h^2-acetate species, where the coverage of reactively formed h^2-acetate species increases with decreasing gold concentration similar to the

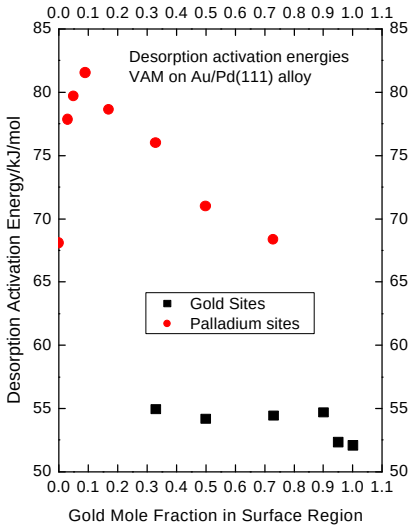

Figure 12: The desorption activation energy for of vinyl acetate on various Au/Pd(111) alloys surface plotted versus gold mole fraction in the near-surface region for desorption from gold (■) and palladium (●) sites.

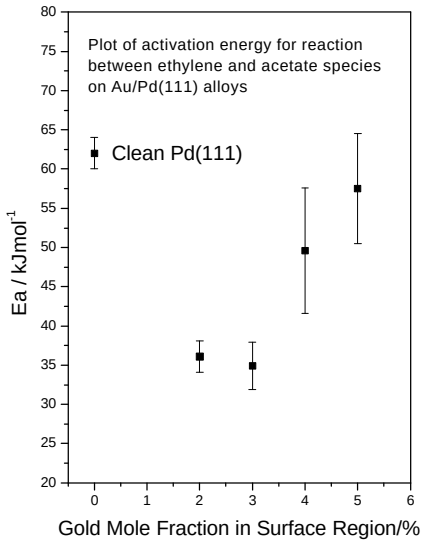

Figure 13: Plot of the activation energy for ethylene reaction with acetate species to form vinyl acetate on various Au/Pd(111) alloys.

chemistry seen on clean Pd(111) [32,33]. Pd appears to be necessary in order to activate acetic acid to acetate.

Preliminary experiments have also been carried out on the surface chemistry of vinyl acetate on gold-palladium alloys. At high gold mole fractions, vinyl acetate desorbs molecularly from both gold and palladium sites. As the palladium coverage increases, a larger proportion of the vinyl acetate decomposes in a similar manner to that shown in Fig. 10. However, molecular vinyl acetate desorption is detected from surfaces with all alloy compositions. The resulting desorption activation energies of VAM from gold (■) and palladium (●) sites on a Au/Pd(111) alloy are shown in Fig. 12 as function of gold mole fraction in the near-surface region. This suggests that the heat of adsorption increases when gold is added to the surface. This curious result is currently being explored using theory.

The reaction rate between acetate and ethylene was measured for various alloy compositions as a function of the mole fraction of gold in the near-surface region and the preliminary results are plotted in Fig. 13. This reveals that a relatively small amount of gold in the alloy, only a few percent, decreases the activation energy for insertion into adsorbed acetate species by a factor of about 2. These data are now being analyzed using the alloy coverage measurements described above to identify the surface structures that are responsible for this decrease in reaction activation energy. We are currently extending this work to study Pd(100) surfaces and have collected TPD and XPS data for ethylene, acetic acid and vinyl acetate adsorption on Pd(100) and are currently collecting the infrared data for these systems. This work is of particular interest since the Au/Pd(100) alloy has been identified as being particularly active for the synthesis of vinyl acetate [34,35] and these experiments are aimed at understanding the origin of these effects. Once these experiments are complete, we will grow alloys on these surfaces and characterize them using the strategies outlined above.

1. (D) Denisty Functional Theory on Au/Pd Alloy Surfaces

We have carried out a number of detailed density functional theoretical calculations in order to determine the adsorption energies, overall reaction energies, and activation barriers for both the selective pathways that lead to VAM synthesis as well as the unselective paths that lead to surface carbon, ethylidyne, CO_2 and other unselective products over a systematic series of Pd, Au and PdAu alloy surfaces. Most of the theoretical results, as discussed above, were focused on understanding the chemistry over the Pd(111) surface in order to compare with experimental results. In addition, we have begun to explicitly examine the influence of lateral interactions that occur between co-adsorbed intermediates as the surface coverage is increased and their influence on the sites for adsorption and reaction, along with their effects on the overall reaction energies

and activation barriers. A summary of some of the calculated results at both high and low coverages are presented in Table 1 and Fig. 14 (where the direction of the arrows indicate increasing reactant coverage). The results are consistent with those reported above, predicting that the mechanism proceeds via the Samanos route. Ethylene activation over Pd is difficult especially at higher surface coverages and more readily reacts directly with adsorbed acetate at higher coverages to form the acetoxyethyl intermediate. The acetoxyethyl intermediate subsequently undergoes a β-hydride elimination to form VAM. At higher oxygen coverages, the acetoxyethyl can also react by transferring the β-hydrogen to the adsorbed oxygen. We have calculated the effects of coverage on the reaction energies and the activation barriers for various reactions by co-adsorbing oxygen and/or acetate at increasing levels. The results for many of the reaction steps show that they roughly follow an Evans-Polanyi relationship (Fig. 14). This thus provides a more rapid way to determine the effects of coverage on the activation energies for specific reactions. We will complete these same calculations for all of the steps outlined in Table 1.

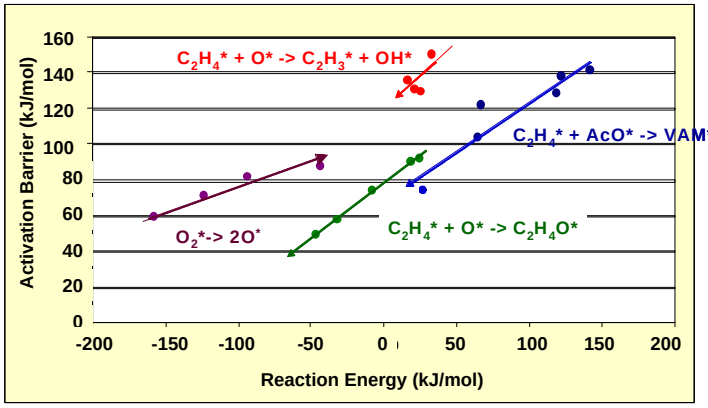

Figure 14: DFT calculated Evans-Polanyi relationships demonstrating the influence of coverage on the reaction energy and its influence on the corresponding activation energy.

The results reported here clearly show that the surface coverage can significantly influence the activation barriers for different elementary steps. As might be expected, the barriers for bond-breaking reactions increase, whereas the barriers for bond-making reactions decrease. The barrier for ethylene coupling (bond making), for example, is reduced by nearly 45 kJ/mol, while the subsequent barrier for VAH activation (bond breaking), is increased by 20 kJ/mol. Simulations reveal that while increasing the coverage accelerates the rate for ethylene coupling with acetate, ethylene adsorption is also quite critical since acetate and oxygen block the surface and act to limit the availability of open sites for ethylene to adsorb. These results were subsequently used in order to help develop an ab initio-based, kinetic Monte Carlo simulation code by which we can examine the influence of the metal, as well as operating conditions on the surface chemistry.

As was discussed earlier, we previously suggested from preliminary calculations that the active sites for VAM formation over PdAu alloys consisted of Pd ensembles on the order of 3-5 Pd atoms surrounded by Au. In a very interesting recent study, Goodman demonstrated that non-contiguous Pd pairs, formed within the surface of the Au(100) substrate, demonstrated very high selectivities as well as enhanced activities [34,35]. They suggested that Au acts to prevent the reactions responsible for surface carbon formation. This improves both the selectivity as well as the activity. A model of this Pd_2Au_2/Au(100) surface is displayed in Fig. 15.

The detailed analysis of the surface structure in this system provided an excellent starting point for theory. We therefore calculated the adsorption energies, overall reaction energies, and activation barriers for reactions on this surface to compare with the results on Pd before moving onto unknown PdAu alloys. The calculations for this system were carried out at lower coverages as this was thought to be the likely situation under reaction conditions. (Ultimately, our kinetic Monte Carlo simulations will allow us to establish the appropriate steady-state surface coverages to examine with theory). The DFT-calculated activation barriers for the critical steps for VAM formation over this surface are shown in direct comparison with those for the pure Pd(111) substrate in Table 2 below.

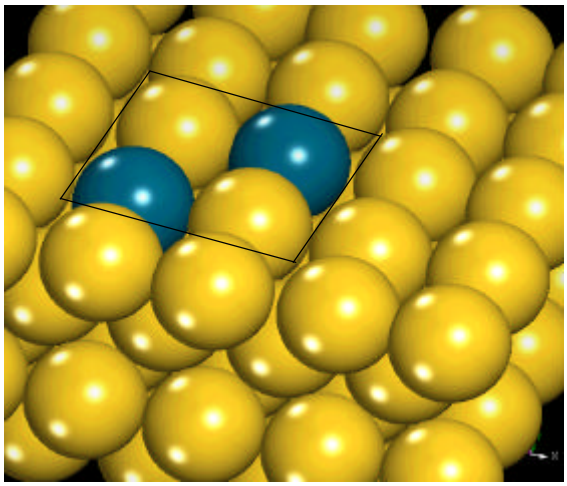

Figure 15. The highly selective and active Pd_2Au_2/Au(100) surface for VAM synthesis, from Goodman *et al* [34,35].

The calculated barriers indicate that there is a change in the reaction mechanism from that found over Pd(111) [19,36]. Despite the high gold coverage, molecular oxygen can still dissociate on these surfaces as the result of the non-contiguous Pd pairs, which provide Pd atoms within the two bridge sites across the four-fold

Reactions	**0 ML**	**Limit**	**0.25 ML**		**0.6 ML**
	ΔE_{RXN}	ΔE_a	ΔE_{RXN}	ΔE_a	ΔE_a
C_2H_4* + AcO* => VAH*	82.6	161.1	82.3	112.6	73.0
C_2H_3* + AcO* => VA*	19.1	102.9	-11.8	72.1	106.2
VAH* + O* => VA* + HO*	-43.9	48.8	-40.3	28.6	34.7
O_2* => 2 O*	-189.2	51.1	-185.9	18.6	84.0
C_2H_4* + O* => C_2H_3* + HO*	19.6	152.9	29.3	147.9	124.5
C_2H_4* + O* => CH_2CH_2O*	54.6	130.1	49.7	125.3	47.3
C_2H_3* + O* => CH_2C* + HO*	-27.4	134.0	-61.6	83.6	
C_2H_3* + O* => C_2H_2* + HO*	-22.7	115.8	-71.3	51.9	
C_2H_3* + O* => CH_2CHO*	17.1	140.7	-17.9	105.8	
C_2H_3* + O* => $CHCH_2O$*	35.4	154.1	-29.1	89.6	
C_2H_3* => CH_2* + CH*	12.3	139.5	27.7	139.5	
CH_2CH_2O* + O* => CH_2CHO* + HO*	-17.9	98.9	-106.3	36.9	
CH_2CH_2O* + O* => CH_2OCH_2O*	-14.0	147.1	-73.1	88.0	
CH_2CHO* + O* => CHCHO* + HO*		105.7	1.0	112.0	
CH_2CHO* + O* => CH2OCHO*	-4.0	138.1	-20.6	121.7	
CH_2CH_2OH* + O* => CH_2CHOH* + HO*	-71.8	75.2	-67.8	51.0	
CH_2CH_2OH* + O* => CH_2OCH_2OH*	-13.1	114.3	-43.2	83.7	

Table 1: DFT calculated overall reaction energies and activation barriers for some of the elementary steps proposed for VAM synthesis over the Pd(111) at different surface coverages.

hollow site. Oxygen can dissociate over the 4-fold hollow site allowing the two oxygens to bind to the resulting Pd-Au bridge sites. The atomic oxygen that forms is weakly bound and quite basic thus making it very highly reactive. It readily activates the C-H bond of ethylene thus promoting the Moiseev mechanism. The rate-limiting step on these surfaces now becomes the coupling of the more strongly bound vinyl (as opposed to the weakly held ethylene) with acetate on the surface.

REACTIONS	Pd_2Au_2/Au(100)		Pd_2Au_2/Au(100)		Pd(111)
	0 ML	Coverage	0.25 ML	Coverage	0.6 ML
	ΔE_{RXN}	ΔE_a	ΔE_{RXN}	ΔE_a	ΔE_a
$O_2 = 2O^*$	7.6	38.4	37.4	53.4	18.3
$AcO^* + C_2H_4^* = VAH^*$	62.4	122.1	97.0	117.8	67.6
$VAH^* = VA^* + H^*$	-6.00	50.9	-15.5	36.9	62.7
$VAH^* + O^* = VA^* + HO^*$	-143.4	20.5	-158.9	1.4	38.6
$C_2H_4^* = C2H3^* + H^*$	82.5	133.1	108.2	133.7	135.1
$C_2H_4^* + O^* = C_2H_3^* + HO^*$	-54.9	62.4	-13.5	66.1	115.8
$AcO^* + C_2H_3^* = VA^*$	-26.1	130.6	-32.5	80.6	106.2

Table 2: A comparison of the reaction energies and the activation barriers for the elementary steps in VAM synthesis for the Pd_2Au_2/Au(100) surfaces proposed by Goodman [34,35] at low coverages and for the Pd(111) surface at high coverage.

Preliminary experiments on the gold palladium alloy reveal that there is no deuterium isotope effect as found on clean Pd(111) (Fig. 7) suggesting that there is indeed a switch in reaction pathways on alloy surfaces. The addition of Au to the surface weakens the bonds of both acetate and vinyl intermediates, which reduces carbon formation thus preventing carbon accumulation on the surface. In addition, the high concentration of Au about the contiguous Pd sites leads to few neighboring adsorbates and results in low local surface coverages. The lower coverage acts to reduce the number, as well as the strength of adsorbate-adsorbate interactions, which decreases the overall lateral repulsive interaction energy. The significant decrease in adsorption energies for the surface intermediates that was found for the high-coverage, pure palladium surface does not occur on this predominantly Au surface. The activation barriers for bond-making reactions such as the coupling of vinyl and acetate at these sites are therefore increased on the high-gold coverage alloy surfaces. There is clearly a delicate balance that must exist between the incorporation of Au into the surface, which *reduces* the adsorption energies of surface intermediates, while at the same time reducing their lateral interactions, which *increases* their binding energies. This is born out by the higher barriers reported for ethylene coupling with acetate on the Pd_2Au_2/Au(100) surface. These surfaces, however, are still likely to be more active than Pd alone as they significantly lower carbon poisoning. We are currently working to incorporate this kinetic data into the KMC simulations to elucidate the rates for comparison.

Both the Pd(111) and the Pd_2Au_2/Au(100) alloy proposed by Goodman present well-defined model surfaces. The surfaces alloys that were formed and used to generate the results in Figs. 14 and 15 must clearly contain a distribution of different PdAu compositions and surface ensembles. In order to model these systems, it is essential to obtain a more complete understanding of the influence of alloying and surface coverage effects on the elementary reaction energetics. To that end we have carried out a broad range of calculations on Pd(111), Pd(100), Au(111), Au(100) surfaces as well as on different model PdAu alloys and bimetallics in order to examine in detail the electronic, geometric and lattice-strain effects on the adsorption energies, overall gas-phase reaction energies and activation barriers. The results reveal that the ensemble or geometric effects that result from alloying Au into the Pd surface are quite large. There is reduction in the adsorption energy that is on average 40-80 kJ/mol for just the addition of just one

Pd 111	bare	1 Ligand	all Ligands	1 SS	all SS	overlayer	2 OL
AcO (ds)	-206.93	7.16	20.71	-1.59	17.02	-10.73	-33.80
C2H3 (pi)	-249.93		37.35	-1.53	24.77	1.46	-37.02
C2H3 (ts)	-264.05	11.66	47.73	-1.57	25.27	16.44	-28.85
C2H4 (ds)	-87.06	9.85	35.16	-3.53	14.28	6.62	-21.36
C2H4 (pi)							
C (fcc)	-650.73	4.86	40.21	-0.55	25.46	-6.31	-69.58
CCH3 (hcp)	-540.30	6.19	40.18	2.36	22.83	14.32	-27.70
CHCH3 (b)	-336.71	9.72	56.76	0.48	17.23	17.81	-17.37
CO (b)	-182.25		40.30	-0.34	0.00	0.88	-22.55
CO (fcc)	-202.60	4.41	19.47	-1.35	10.88		
H (hcp)	-275.64	2.55	10.69	0.69	1.94	-5.49	-10.05
HO (b)	-232.94	9.10	31.10	-0.62	19.36		
O (hcp)	-386.39	7.72	41.79	-0.77	21.09		
average	0.00	7.32	35.12	-0.69	18.19	3.89	-29.81

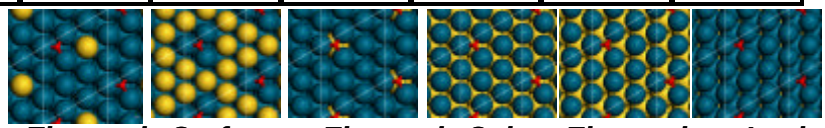

Electronic Surface Effects ***Electronic Sub Surface Effects*** ***Electronic vs. lattice Expansion*** ***Lattice Expansion***

Table 3: DFT calculated lateral interactions for different adsorbates on different alloys. The results systematically explore the different electronic effects as well as lattice expansion effects. Positive numbers refer to repulsive interactions whereas negative values refer to attractive interactions. Energies are in kJ/mol.

Au atom into the adsorbate-surface complex. The relative weakening of the adsorbate interaction strength appears to increase linearly with the number of Au atoms in the actual adsorption site. The binding energy for a carbon atom, for example, decreased by nearly 200 kJ/mol upon the creation of a well-defined Pd_2Au_1 surface alloy.

The electronic effects that result are much weaker than the geometric effects. The electronic effects for adding one neighboring Au atom decreased the binding energies by about

10.6 kJ/mol on average. Both surface and subsurface Au in direct contact with Pd appear to lead to charge transfer from Au to Pd, thus weakening adsorbate bonding on Pd sites. The exception to this occurs when Au itself is the substrate. The Au substrate (which has a lattice constant of 2.81 Å) leads to a lattice expansion of the Pd surface layer, which in turn induces strain in the Pd surface. This ultimately increases the binding for most adsorbates on the Pd surface. We have developed a rather extensive database of adsorption energies, reaction energies and, in a number of cases, activation barriers. A small snapshot of the data on just on the electronic effects of alloying Au into the Pd(111) surface is presented in Table 3. In addition, we have also examined Au into Pd(100), Pd into Au(111) and Pd into Au(100).

The database is being used to construct structure-property relationships, which show how the surface coverage, process conditions, and alloy configuration all affect the actual reaction energies and barriers and, as such, the reaction rate and selectivity. Most of our preliminary work discussed so far has focused on using theory to calculate the reaction energetics, including adsorption energies, reaction energies and activation barriers. The simulation of the kinetics, however, also requires pre-exponential factors in order to appropriately account for the rate. In our initial simulations, we used simple statistical mechanics in order to estimate the pre-exponential factors for different reactions and surface processes. We are currently calculating the entropic changes between the transition state and the reactant state within the harmonic approximation for the specific reaction steps discussed earlier in order to calculate the pre-exponential factors. We are finding that it is important to include anharmonicity. The ability to appropriately model the pre-exponential factors is still an emerging area of research as it is very difficult to fully separate out the low-frequency modes induced by the metal. The low frequency modes that result, if incorrect, will significantly reduce the accuracy of the kinetics. Theory will be used to establish the partition functions, calculate pre-exponential factors and compare them with typical values from statistical mechanics for all of the elementary processes of interest.

In order to fully compare theory with experiment, we will also need to be able to establish the surface composition, specific atomic configuration within each layer of the alloy. We will therefore carry out a number of additional calculations over a range of possible thermodynamic configurations. The results will be used in order to construct binary alloy phase diagrams in order to establish the lowest energy phases. In addition, the ab initio results determined thus far have been used to construct ab-initio-based embedded atom potentials. They are currently being used to carry out simulated annealing studies to establish the different alloys we will follow. The results will be used in the ab initio kinetic Monte Carlo simulation developed in order to simulate temperature programmed desorption profiles for a distribution of the most favorable surface alloys in order to compare with those determined experimentally using results from LEIS, LEED I/E curves and STM experiments as described above.

References

1. U.S. Patent number 365888, 1967
2. K. Luo, T. Wei, C.W. Yi, S. Axnanda and D.W. Goodman, *J. Phys. Chem., B* **109,** 23517 (2005)
3. C.J. Baddeley, M. Tikhov, C. Hardacre, J.R. Lomas and R.M. Lambert, *J. Phys. Chem. B.*,

100, 2189 (1996)
4. R.M. Ormerod, C.J. Baddeley and R.M. Lambert, *Surf. Sci.*, **259,** L709 (1991)
5. W. F. Egelhoff, Jr., *Surf. Sci. Rep.*, **6,** 253 (1987)
6. Z. Li, O. Furlong, F. Calaza, L. Burkholder, H. C. Poon, D. Saldin and W. T. Tysoe, *Surf. Sci.*, submitted
7. F. Maroun, F. Ozanam, O. M. Magnussen, and R. J. Behm, Science 293, 1811 (2001)
8. M. Ruff, Ph.D. thesis, Universität Ulm, (2000)
9. Dingwang Yuan , Xingao Gong, and Ruqian Wu, Phys. Rev. B **75,** 087428 (2007)
10. J. A. Boscoboinik, C. Plaisance, M. Neurock and W. T. Tysoe, *Physical Review B,* submitted
11. T. Zheng, D. Stacchiola, D.K. Saldin, J. James, D.S. Sholl and W.T. Tysoe, *Surf. Sci.*, **574,** 166 (2005)
12. Joanna James, Dilano K. Saldin, T. Zheng, W. T. Tysoe and David S. Sholl, *Catal. Today,* **105,** 74 (2005)
13. H. C. Poon, M. Weinert, D. K. Saldin, D. Stacchiola, T. Zheng and W. T. Tysoe, *Phys. Rev. B.* **69,** 035401 (2004)
14. T. Zheng, D. Stacchiola, H.C. Poon, D.K. Saldin and W.T. Tysoe, *Surf. Sci.*, **564**, 71 (2004)
15. B. Samanos, P. Boutry and R. Montarnal, *J. Catal.*, **23,** 19 (1971)
16. V. Pallassana, M. Neurock, V.S. Lusvardi, J.J. Lerou, D.D. Kragten and R.A. van Santen, *J. Phys. Chem. B.* **106,** 1656 (2002)
17. F.L. Moiseev and M.N. Vargaftik, In *Perspectives in Catalysis, Chemistry for the 21st Century* Thomas, J.M., Zhamoriov. A. Eds.; Blackwell Science, 1992, p 91
18. Dario Stacchiola, Florencia Calaza, Luke Burkholder and Wilfred T. Tysoe, *J. Am. Chem. Soc.*, **126,** 15384 (2004)
19. D. Stacchiola, F. Calaza, L. Burkholder, A. W. Schwabacher, M. Neurock and W. T. Tysoe, *Angew. Chem.*, **44,** 4572 (2005)
20. R.J. Koestner, M.A. Van Hove and G.A. Somorjai, *J. Phys. Chem.*, **87,** 203 (1983)
21. L.L Kesmodel, L.H. Dubois and G.A. Somorjai, *Chem. Phys. Lett.*, **56,** 267 (1978)
22. P.Cremer, C. Stanners, J. Neimantsverdreit, Y. Shen and G.A. Somorjai, *Surf. Sci.*, **328,** 111 (1995)
23. P.Cremer and G.A. Somorjai, *J. Chem. Soc., Faraday Trans.*, **91,** 3671 (1995)
24. P. Cremer, X. Su, Y. Shen and G.A. Somorjai, *J. Am. Chem. Soc.*, **118,** 2942 (1996)
25. P. Cremer, X. Su, Y. Shen and G.A. Somorjai, *Catal. Letts*, **40,** 143 (1996)
26. M. Kaltchev, A.W. Thompson and W. T. Tysoe, *Surf. Sci.*, **391,** 145 (1997)
27. J. Bellamy, *Infrared Spectra of Complex Molecules* (Wiley, New York, 1964)
28. F. Calaza, D. Stacchiola M. Neurock and W. T. Tysoe, *Surf. Sci.*, **598,** 263 (2005)
29. E.M. Stuve and R.J. Madix, *J. Phys. Chem.*, **89,** 3183 (1985)
30. F. Calaza, F. Gao, Z. Li and W.T. Tysoe, *Surf. Sci.*, **601,** 714 (2007)
31. Z. Li, F. Calaza, F. Gao and W.T. Tysoe, *Surf. Sci.*, **601,** 1351 (2007)
32. J.L. Davis and M.A. Barteau, *Surf. Sci.*, **256,** 50 (1991)
33. R.D. Haley, M.S. Tikhov and R.M. Lambert, *Catal. Letts.*, **76,** 125 (2001)
34. M.S. Chen, K. Luo, T. Wei, Z. Yan, D. Kumar, C.W. Yi and D.W. Goodman DW, *Catal.*

Today, **117,** 37 (2006)
35. M.S. Chen, D. Kumar, C.W. Yi and D.W. Goodman, *Science*, **310,** 291 (2005)
36. E. Hansen and M. Neurock, *J. Phys. Chem. B.*, **105,** 9218 (2001)

2. List of Publications Acknowledging DOE Support

1. Vinyl Acetate Formation By the Reaction of Ethylene with Acetate Species on Oxygen-Covered Pd(111), Dario Stacchiola, Florencia Calaza, Luke Burkholder and **Wilfred T. Tysoe**, *Journal of the American Chemical Society*, **126,** 15384 (2004)

2. Structure and Binding Site of Acetate on Pd(111) Determined Using Density Functional Theory and Low Energy Electron Diffraction, Joanna James, Dilano K. Saldin, T. Zheng, **W. T. Tysoe** and David S. Sholl, *Catalysis Today*, **105,** 74 (2005)

3. On the Reaction Mechanism for the Formation of Vinyl Acetate by the Reaction of Ethylene with Acetate Species on Palladium(111), D. Stacchiola, F. Calaza, L. Burkholder, A. W. Schwabacher, **M. Neurock** and **W. T. Tysoe**, *Angew. Chem.*, **44,** 4572 (2005)

4. Structure and Decomposition Pathways of Vinyl Acetate on Pd(111), Florencia Calaza Dario Stacchiola, **M. Neurock** and **Wilfred T. Tysoe**, *Surface Science*, **598,** 263 (2005)

5. Probing Elementary Steps Under Reaction Conditions Using Infrared Spectroscopy, D. Stacchiola, F. Calaza, L. Burkholder, A. W. Schwabacher, **M. Neurock** and **W. T. Tysoe**, *Ciencia*, **14,** 189 (2006)

6. The Adsorption of Ethylene on Au/Pd(111) Alloy Surfaces, F. Calaza, F. Gao, Z. Li and **W.T. Tysoe**, *Surf. Sci.*, **601,** 714 (2007)

7. The Adsorption of Acetic Acid on Au/Pd(111) Alloy Surfaces, Z. Li, F. Calaza, F. Gao and **W.T. Tysoe**, *Surf. Sci.*, **601,** 1351 (2007)

8. Formation and Characterization of Au/Pd Surface Alloys on Pd (111), Zhenjun Li, Feng Gao, Yilin Wang, Florencia Calaza, Luke Burkholder and **Wilfred T. Tysoe**, *Surf. Sci.*, **601,** 1898 (2007)

9. Probing Reaction Pathways on Model Catalyst Surfaces: Vinyl Acetate Synthesis and Olefin Metathesis, Feng Gao, Yilin Wang, Florencia Calaza, Dario Stacchiola and **Wilfred T. Tysoe**, *Journal of Molecular Catalysis: A Chemical*, in press

10. Surface Chemistry of Acetic Acid on Clean and Oxygen Covered Pd(100), Zhenjun Li, Feng Gao and **W.T. Tysoe**, *Surf. Sci.*, submitted

11. Monte Carlo and Density Functional Theory Analysis of the Distribution of Gold and

Palladium Atoms on Au/Pd(111) Alloys, Jorge A. Boscoboinik, Craig Plaisance, **Matthew Neurock** and **Wilfred T. Tysoe**, *Physical Review B*, submitted

12. Surface Segregation of Gold on Au/Pd(111) Alloys Measured by Low-energy Electron Diffraction and Low-energy Ion Scattering, Zhenjun Li, Octavio Furlong, Florencia Calaza, Luke Burkholder, Hin Cheuk Poon, Dilano Saldin and **Wilfred T. Tysoe**, *Surf. Sci.*, Submitted

3. Financial Statement

No unobligated funds are anticipated at the end of the funding period.